

Simulation and optimization of CNC cylindrical grinder Performance based on equivalent analysis of joints spring-damping characteristics

Mingzheng Qi¹, Han Wang^{1,*}, Xizhi Sun², Tianjian Li¹, Yang Guo¹, and Tao Wu^{3,*}

¹ School of Mechanical Engineering, University of Shanghai for Science and Technology, Shanghai 200093, China

² Department of Mechanical and Aerospace Engineering, Brunel University London, Uxbridge UB8 3PH, UK

³ R&D Centre, Wuhan Second Ship Design & Research Institute, Wuhan 430205, China

Received: 19 October 2024 / Accepted: 19 February 2025

Abstract. This paper focuses on the MKE1620A CNC cylindrical grinder, using an equivalent analysis of the joint spring-damping characteristics to investigate the overall performance of the grinder and propose directions for design optimization. A total of 168 spring-damper elements were established to model the fixed, movable, and bearing joints. These elements were classified and calculated to determine their parameters, which were then incorporated into a finite element analysis model to examine the impact of joint stiffness on the static and dynamic performance of the machine tool, with results showing less than a 10% error compared to actual measured data. Additionally, the paper investigates how the quality of six common structural materials influences the first-order natural frequency of components and explores the relationship between variations in joint stiffness and changes in the machine tool's natural frequency. The findings provide theoretical and data-driven insights for the design and optimization of CNC cylindrical grinding machines, serving as a valuable reference for enhancing machine tool performance and machining quality.

Keywords: CNC cylindrical grinding machines / joints stiffness / spring-damping characteristics / performance simulation

1 Introduction

The demands for high efficiency, high speed, and high precision in modern machining are increasing, putting higher requirements on machine tool performance. Traditional design methods involving physical prototype trial production, testing, and optimization are costly and time-consuming, and no longer meet the needs of modern machine tool design. With the development of computer simulation technology, it has been widely used in the design of machining equipment, addressing the challenges posed by the increasing performance requirements of products and meeting the demands of shorter development cycles in market competition. It allows for the design and manufacture of high-quality machine tools in the shortest time while minimizing design costs.

Joints modelling is an important research area in machine tool simulation, involving disciplines such as multi-body dynamics, computational methods, and software engineering [1,2]. Guo et al. [3] modeled the dynamics of the

fixed spindle joints of machine tools based on virtual material layers and twin finite element models. Wang et al. [4] proposed an optimization method for overall stiffness based on Taguchi experiments, finite element methods, and grey relational analysis for designing the optimal structure of a CNC horizontal machining center (HMC). Chang et al. [5] proposed interfacial micromechanics model to characterize the contact behaviors of bolted joints in an ultra-precision machine tool. This paper aims to explore the overall structure and basic theory of simulation analysis of CNC cylindrical grinders through joint modeling, analyze the equivalent stiffness of the joints, study the impact of component mass on the machine tool's dynamic characteristics, and carry out design and optimization to improve machine tool performance and machining quality.

The spring-damper model is one of the earliest proposed and most widely applied equivalent analysis models for contact surfaces [6]. In this model, spring and damper elements are used to describe the stiffness and damping characteristics of contact surfaces. Yoshimura [7] designed experiments to measure and plot the equivalent stiffness and damping values of contact surfaces under normal pressure per unit area, establishing a database of equivalent stiffness

*Corresponding authors: wangh9@usst.edu.cn;
thewutao@163.com

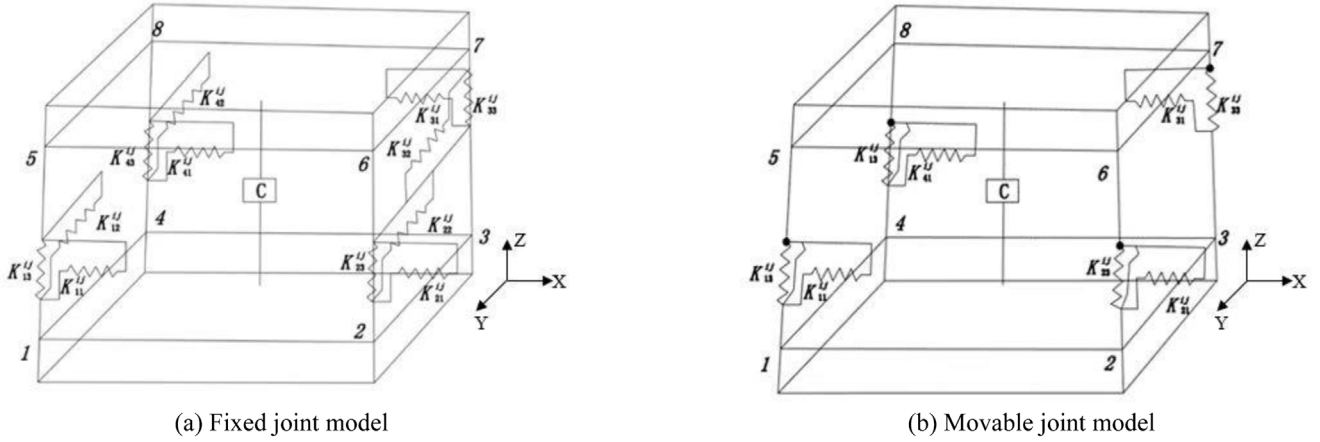


Fig. 1. Equivalent models of fixed and movable joints.

and damping values under various contact conditions. Dogariu et al. [8] adopted a finite element analysis method to design the spindle system of a machine tool, focusing on the dynamic characteristics of the spindle bearing system, and used spring and damper elements to simulate the bearing support mechanism. Chen et al. [9] developed a two-degree-of-freedom stiffness model of a spindle system that accounts for rotor oscillation, based on a spring-damping unit, in their study of a hydrostatic electric spindle system for grinding machines. Revanasiddesh et al. [10] set the boundary condition between the bed and the ground as springs with bolted stiffness to better determine the dynamic performance of the structure during the bed's modal analysis phase. Guo et al. [11] developed a spring-damper model at the weak point of the machine structure to simulate the vulnerable part of the machine structure. Liu et al. [12] conducted a study to accurately identify the contact parameters of joint interfaces in order to improve the machining precision of machine tools based on joint simulations in MATLAB and ANSYS. Wu et al. [13] calculated the stiffness of the joint bearing of the rotary table system, and analyzed the effect of bearing clearance and external load on the stiffness. Gao [14], Song [15], and others conducted research on various types of contact surfaces. They established theoretical models for normal contact of joints, as well as dynamic analysis models for fixed and movable joints, providing computational solutions for addressing joints issues. Altintas et al. [16] created a high-efficiency, reduced-order multibody dynamics model for a five-axis machine tool by incorporating flexible spring and damper elements into the joints that influence machining performance. In summary, the spring-damper model is a theoretically derived model that helps accurately determine the dynamic characteristics of joints.

2 Mathematical modeling of joints

Common joints in CNC cylindrical grinders include:

- Fixed joints: These involve the bolted connections between the bed and the grinding wheelhead guide rail, as well as the connection parts of the headstock and tailstock, which are securely clamped to the worktable.

- Movable joints: These consist of the linear guide contacts between the worktable and machine bed, and between the wheelhead and its guide rails.
- Bearing joints: These include the bearings between the headstock spindle and headstock housing, as well as between the wheelhead spindle and wheelhead housing.

The dynamic characteristics of these joints vary significantly, requiring different types, quantities, and directions of spring-damping elements.

2.1 Modeling of fixed and movable joints

A fixed joint has one normal stiffness and one normal damping coefficient, and two tangential stiffnesses and two tangential damping coefficients, resulting in three stiffnesses and three damping coefficients in total. This can be equivalently represented by three spring-damper elements, with each element corresponding to the normal and tangential stiffnesses and damping coefficients between a pair of joint points. Movable joints release the degree of freedom in the direction of motion, with stiffnesses and damping coefficients demonstrating in two directions (one normal and one tangential). Thus, a pair of movable joint points can be modeled as two spring-damping elements, corresponding to normal and tangential stiffnesses and damping coefficients. The models of fixed and movable joints are shown in Figure 1.

The dynamic load on a joint can be decomposed into forces along six degrees of freedom. Using the Yoshimura Mitsutaka method, integrals are performed over the area represented by each joint point, applying equations (1) and (2) to calculate the equivalent stiffness and damping coefficients of the joint in all directions.

$$\left. \begin{aligned} K_x &= \iint k_1(P_n) dx dz = K_Z \\ K_y &= \iint k_2(P_n) dx dz \\ K_{\theta y} &= \iint (y^2 + z^2) k_1(P_n) dx dz \\ K_{\theta x} &= \iint z^2 k_2(P_n) dx dz \\ K_{\theta z} &= \iint y^2 k_2(P_n) dx dz \end{aligned} \right\} \quad (1)$$

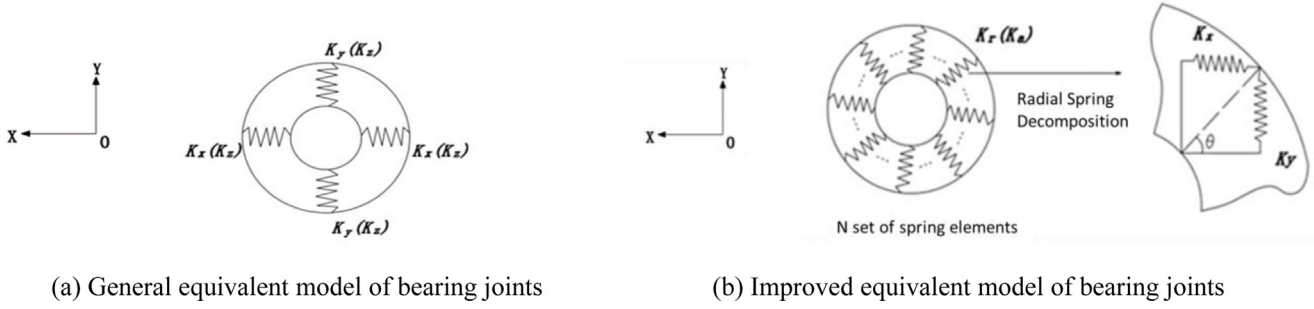


Fig. 2. Equivalent model of bearing joints.

where K represents the joint stiffness, and x , y , z , and θ_x , θ_y , θ_z represent the six degrees of freedom.

$$\left. \begin{aligned} C_x &= \iint c_1(P_n) dx dz = C_z \\ C_y &= \iint C_2(P_n) dx dz \\ C_{\theta_y} &= \iint (y^2 + z^2) C_1(P_n) dx dz \\ C_{\theta_x} &= \iint z^2 c_2(P_n) dx dz \\ C_{\theta_y} &= \iint y^2 c_2(P_n) dx dz \end{aligned} \right\} \quad (2)$$

where c represents the damping of the joint.

2.2 Modeling of bearing joints

Bearing joints involve the interaction between the rolling elements and raceways within the bearing, the connection between the inner ring and spindle, and the connection between the outer ring and support housing. In this study, the bearing's substructure is treated as a whole, considering only the overall effect exhibited by the joint. The basic equivalent model is shown in Figure 2.

Based on the motion and loading of the spindle, the bearing joints are typically modeled using four sets of spring elements evenly distributed on the spindle structure. For simulations requiring higher accuracy, the number of evenly distributed springs can be increased. The damping coefficient of bearing joints, assuming oil lubrication, is approximately calculated using equation (3).

$$C = \frac{24\pi\alpha\eta_0 r^3}{(2rh_0)^{1.5}} \quad (3)$$

where η_0 – the viscosity of the lubricant, assumed to be constant; α – the contact angle between the rolling elements and the outer bearing ring; r – the radius of the rolling elements; h_0 – the thickness of the lubricant film.

The stiffness of the bearing joints K is determined by the stiffness between the outer ring and ball, K_{ko} , and the stiffness between inner ring and ball, K_{ki} . The stiffness of the bearing joints K can be calculated

approximately using Hertz contact theory as shown in equation (4).

$$\left. \begin{aligned} K_{ki} &= 2.15 \times 10^5 \sum \rho_i^{-\frac{1}{2}} (\delta_{ki}^*)^{\frac{3}{2}} \\ K_{ko} &= 2.15 \times 10 \sum \rho_o^{-\frac{1}{2}} (\delta_{ko}^*)^{\frac{3}{2}} \\ K &= \left[\frac{1}{(1/K_{ki})^{2/3} + (1/K_{ko})^{2/3}} \right]^{\frac{3}{2}} \\ K_x &= K \sin \theta \\ K_y &= K \cos \theta \end{aligned} \right\} \quad (4)$$

where, K_{ki} - the stiffness between the inner ring and rolling elements; K_{ko} - the stiffness between the outer ring and rolling elements; $\sum \rho_i$ - the sums of the curvatures of rolling elements and the inner raceway; $\sum \rho_o$ - the sums of the curvatures of rolling elements and the outer raceway; δ_{ki} - contact deformations between rolling elements and the outer ring; δ_{ko} - contact deformations between rolling elements and the inner ring; θ - acute angle between the bearing joint and the x-axis.

3 Simulation model of the CNC cylindrical grinder

The static stiffness of a machine tool affects its machining accuracy and stability. Improving machine stiffness is beneficial for enhancing machining accuracy. For the MKE1620A CNC cylindrical grinder, a finite element analysis model, as shown in Figure 3, was developed to perform static analysis on the entire machine tool. The simplified machine tool model consists of 13 components, including the machine bed, worktable, headstock, tailstock, wheelhead, and wheelhead guide rails which are made of cast iron, headstock spindle, tailstock sleeve, headstock center, tailstock center and wheel spindle. Workpiece are made of steel, and the grinding wheel is made of CBN. The material properties are listed in Table 1.

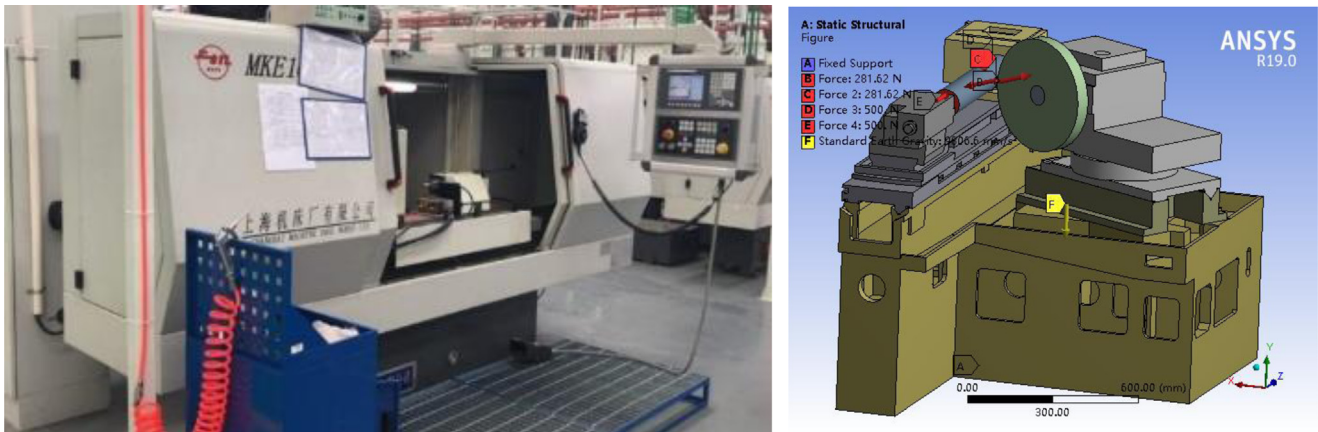


Fig. 3. The MKE1620A CNC cylindrical grinder and the Finite element analysis model.

Table 1. Material properties of structural components.

Material	Young's modulus (GPa)	Poisson's ratio	Density (kg/m ³)
HT300	143	0.27	7300
45 quenched and tempered steel	210	0.3	7850
CBN	7.2	0.2	3480

3.1 Equivalent stiffness of joints

The simplified machine tool model includes fixed joints (such as those connecting the machine bed and wheelhead guide rails, and the headstock to the worktable), movable joints (including the linear guide contact between the worktable and machine bed, as well as between the wheelhead and its guide rails), and bearing joints (such as those between the headstock spindle and headstock housing, along with the bearing joint between the spindle of the wheel frame and the wheel frame housing).

In theoretical calculations and finite element analyses, spring-damper elements are used to model the connection between the two contact surfaces of a joint. Specific coefficients are assigned to the spring-damping elements, enabling theoretical analysis and finite element simulations of the joint and the overall machine system. A key challenge in using spring-damper elements to simulate joints lies in the arrangement and number of these elements. For practical purposes, spring-damper elements are typically established between pairs of hard points (defined as geometric points where mesh nodes are generated). Adding more spring-damping connections between joint surfaces enables more detailed and accurate simulation of joint characteristics.

Considering the actual motion and assembly relationships between the various components, the following approaches are applied to the joints:

- The contact surfaces of the linear guide between the worktable and the machine bed (including flat and V-shaped contact surfaces) are evenly divided into 24 pairs of hard points. Each pair includes one normal spring-damping element and one tangential damping element, resulting in a total of 48 spring-damping elements.

- At the fixed interface between the machine bed and the wheelhead guide rails, eight pairs of hard points are uniformly established. Likewise, eight pairs of hard points are uniformly placed at the fixed interface between the headstock and the clamping surface of the worktable. Additionally, eight pairs of hard points are established at the fixed interface between the tailstock and the clamping surface of the worktable. For each pair of hard points, a normal spring-damper element and two tangential damper elements are represented, resulting in a total of 72 spring-damper elements.
- Sixteen pairs of hard points are evenly distributed at the contact surfaces between the wheelhead and its guide rails (including both flat and V-shaped contact surfaces). Each pair of hard points is represented by a normal spring-damper element and a tangential damper element, resulting in a total of 32 spring-damper elements.
- Four pairs of hard points are uniformly established along the contact surface between the headstock spindle and the headstock housing at the bearing interface. An axial spring-damper element and a radial damper element are applied between each pair of hard points, resulting in a total of 8 spring-damper elements.
- Four pairs of hard points are uniformly established along the contact surface between the wheelhead spindle and the wheelhead housing at the bearing interface. An axial spring-damper element and a radial damper element are applied between each pair of hard points, resulting in a total of 8 spring-damper elements.

At this point, a dynamic equivalent model of the grinding machine tool's entire structure has been established by representing the joints with 72 pairs of hard points. A total of 168 spring-damper elements have been used.

Table 2. Parameters for fixed contact surfaces and movable contact surfaces.

	Contact surface 1 of the joint (Fixed surface)	Contact surface 2 of the joint (Movable surface)	Force/N	Contact area/m ²	Number of spring sets
1	Machine bed	Flat worktable guideway	1698.35	0.07245	12
2	Machine bed	V-shaped worktable guideway	1201	0.04781	12
3	Machine bed	Wheelhead guide rail	3098.18	0.10215	8
4	Worktable	Headstock	659.87	0.05690	8
5	Worktable	Tailstock	382.25	0.03137	8
6	Wheelhead	Flat wheelhead guide rail	1231.5	0.03025	8
7	Wheelhead	V-shaped wheelhead guide rail	1080	0.01945	8

Table 3. Parameter for a single spring-damper element at a fixed joint.

Contact surface 1 of the joint	Contact surface 2 of the joint	Vertical stiffness (N/m)	Shear stiffness (N/m)	Vertical damping (Ns/m)	Shear damping (Ns/m)
Machine bed	Wheelhead guide rail	1.25×10^6	1.25×10^4	1250	1250
Worktable	Headstock	7.13×10^5	7.13×10^3	712.5	712.5
Worktable	Tailstock	1.25×10^6	1.25×10^4	375	375

Table 4. Parameter for a single spring-damper element at a movable joint.

Contact surface 1 of the joint	Contact surface 2 of the joint	Vertical stiffness (N/m)	Shear stiffness (N/m)	Vertical damping (Ns/m)	Shear damping (Ns/m)
Machine bed	Flat worktable guideway	5.8×10^5	5.8×10^3	583	58.3
Machine bed	V-shaped worktable guideway	8×10^5	8×10^3	667	66.7
Wheelhead guide rail	Flat wheelhead guide rail	3.75×10^5	3.75×10^3	375	375
Wheelhead guide rail	V-shaped wheelhead guide rail	5×10^4	5×10^4	50	50

3.2 Calculation of joint parameters

The parameters for fixed joints, movable joints, and bearing joints are obtained through theoretical calculations using equations (1) to (4). First, the contact area and total load for each contact region are calculated. The total load includes the weight of the structure mounted on the contact area and the preload. The corresponding normal stiffness and damping coefficient per unit area, as well as the tangential stiffnesses and damping coefficients per unit area, are derived from the calculated pressure. These values are then integrated over the area represented by each joint point to obtain the equivalent stiffness and damping coefficient in each direction for that joint. The weight of the components, contact area, and the number of spring-damper elements for each joint are listed in Table 2. The stiffness and damping coefficient for a single spring-damper element in fixed joints are provided in Table 3, while those for movable joints are shown in Table 4. The parameters for bearing joints are listed in Table 5.

Table 5. Parameters for each spring element at a bearing joint.

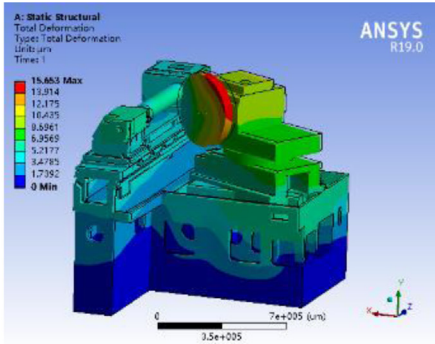
Joints	Axial stiffness (N/m)	Radial stiffness (N/m)
Headstock bearing	1.08×10^6	1.1×10^7
Wheelhead bearing	1.28×10^6	2.3×10^7

4 Analysis of static and dynamic performance of the machine tool

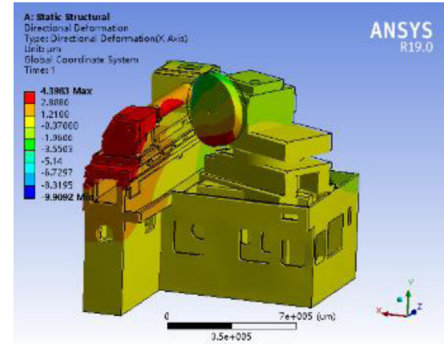
4.1 Static performance of the machine tool

The static stiffness of the entire machine tool is calculated based on static loads, and the deformation contours are shown in Figure 4.

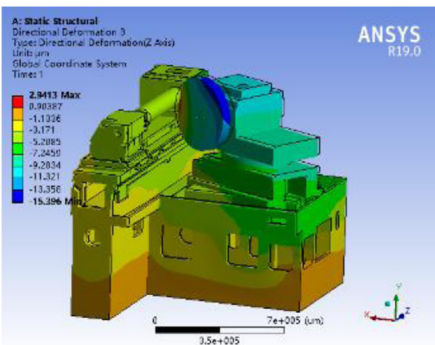
From Figure 4, it can be seen that the maximum deformation in the X direction is concentrated around the tailstock and worktable. The maximum deformation in the Y direction is concentrated in the contact area between



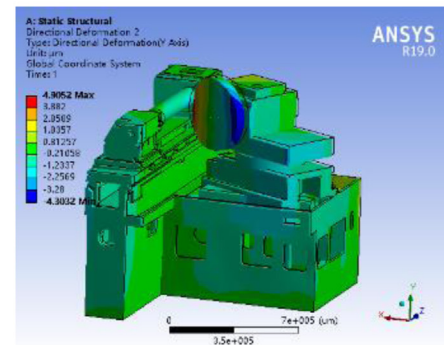
(a) Deformation of the entire machine tool



(b) Deformation in X-direction



(c) Deformation in Y-direction



(d) Deformation in Z-direction

Fig. 4. Deformation maps of the entire machine tool and in the three directions.

Table 6. Static stiffness values in three directions.

	In X direction	In Y direction	In Z direction
Deformation (μm)	4.39	4.9	2.9
Static stiffness ($\times 10^6/\text{N/m}$)	60.82	18.16	3.45

the grinding wheel and the workpiece, while the maximum deformation in the Z direction occurs within the rib of the machine bed. The calculated stiffness values in the three directions are listed in Table 6. As shown in Table 6, the static stiffness of the machine in the X, Y, and Z directions is generally satisfactory, meeting the requirements for grinding machine static stiffness. However, the stiffness in the Z direction is relatively weaker compared to the X and Y directions.

4.2 Dynamic characteristics of the machine tool

The dynamic characteristics of the machine tool are analyzed using modal analysis. By solving the machine tool’s modal parameters, including natural frequencies, modal damping ratios, and mode shapes, the first ten

natural frequencies and mode shapes of the machine tool are obtained. At the same time, the natural frequencies of the machine tool can also be obtained through experimental testing, as shown in Figure 5. A modal test was conducted on the machine bed using a KISTLER PCB piezoelectric triaxial accelerometer, an ALDLINK data acquisition card, and a KISTLER 9728A20000 impact hammer. The natural frequencies of the machine tool’s first six modes are listed in Table 7. The simulation results show that the errors, when compared to the test results, are within 10%.

It can be seen that the most significant vibrations in the machine bed occur at the contact points between the machine bed and the worktable, as well as between the machine bed and the wheelhead guide rail. The most significant vibrations in the wheelhead occur at the



Fig. 5. Experimental testing setup.

top and rear of the wheelhead. The most significant vibrations in higher order modes occur at the headstock and tailstock.

The significant vibration deformation at the grinding wheel is likely related to the material and structure of the grinding wheel and its assembly position. The grinding wheel material, CBN, has a lower modulus of elasticity and density compared to gray cast iron and steel. Additionally, the grinding wheel's radius is much larger than its thickness, and it is mounted on the machine as a large mass cantilever beam structure, resulting in lower local stiffness.

4.3 Effect of component materials on the dynamic characteristics of the entire machine tool

Based on the above dynamic characteristics analysis results, the impact of component material on the dynamic characteristics of the components is analyzed by maintaining the geometric dimensions of the structure and changing the materials of each component. The headstock, tailstock, and wheelhead are assigned six different material: concrete, aluminum, gray cast iron, iron, steel, and copper. The machine bed is assigned five different material: epoxy resin, concrete, granite, aluminum, and gray cast iron. The analysis of how component materials affect the dynamic characteristics of the entire machine tool indicates consistent trends among the headstock, tailstock, and wheelhead. The simulation results for the wheelhead are shown in Figure 6. When the materials for the headstock, tailstock, and wheelhead are set to aluminum, the first ten natural frequencies of the entire machine tool are the highest. When the materials are iron or steel, the first ten natural frequencies of the entire machine tool are also relatively high, and they are higher than those obtained with cast iron.

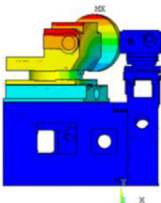
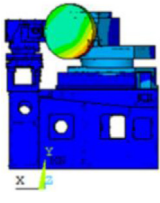
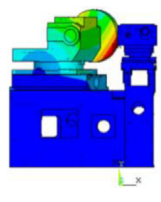
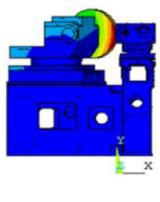
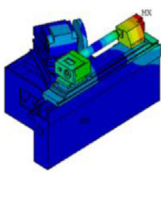
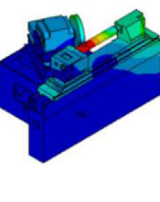
The impact of the machine bed material properties on the frequencies is shown in Figure 7. When the bed material is epoxy resin and the materials of other components remain unchanged, the first ten natural frequencies of the entire machine tool are the lowest. Conversely, when the machine bed material is granite, these frequencies are the highest.

5 Conclusions

Based on the modeling and simulation analysis of the joints of the CNC cylindrical grinder, this study draws the following conclusions:

- Based on the calculation of joint parameters, a more precise finite element analysis model for static and dynamic characteristics has been established, allowing for accurate evaluation of the machine tool's static stiffness and dynamic performances. The results of the static stiffness calculation show that the case machine tool has good static stiffness in the X, Y, and Z directions, meeting the static stiffness requirements for a grinding machine. However, compared to the X and Y directions, the static stiffness in the Z direction is weaker. The dynamic analysis indicates that significant vibration deformation occurs at the grinding wheel, which is related to the material, structure, and assembly position of the wheel. Therefore, special attention should be paid to the material and structure of the grinding wheel during machine tool design process to improve the dynamic characteristics of the machine tool.
- The mass of the components significantly affects the dynamic characteristics of the machine tool. Therefore, selecting the appropriate materials is crucial for improving the performance and machining quality of the machine tool.

Table 7. Comparison of the first ten orders of natural frequency of the machine tool.

Frequency order	Measurement	Differences	Mode shapes	Frequency order	Measurement	Differences	Mode shapes
	Simulation				Simulation		
1	34.6 Hz	10%		4	141 Hz	-8%	
	30.9 Hz				152 Hz		
2	80.8 Hz	2%		5	202 Hz	-8%	
	78.8 Hz				240 Hz		
3	97 Hz	-4%		6	252 Hz	-3%	
	101 Hz				260 Hz		

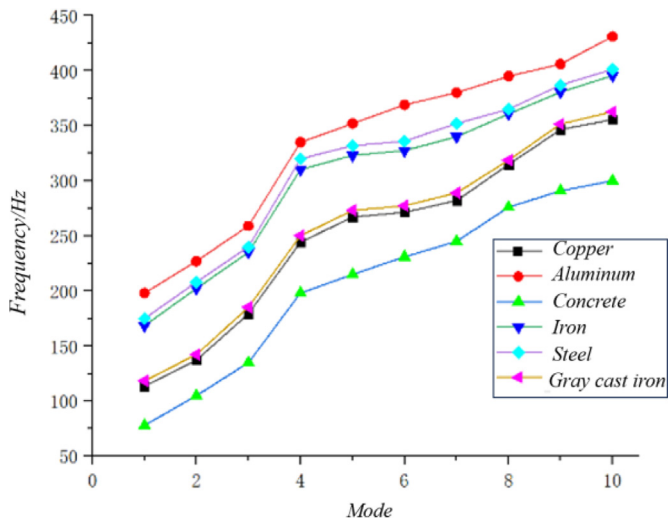


Fig. 6. Relationship between the material of the grinding wheel holder and the frequencies of the entire machine tool.

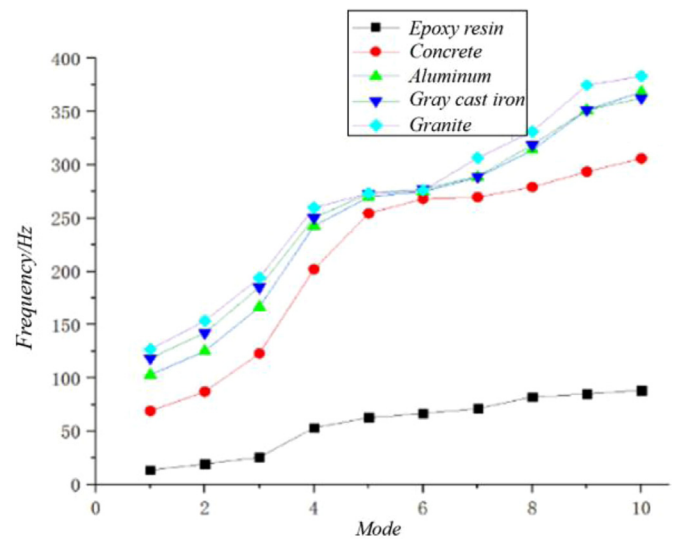


Fig. 7. Relationship between the machine bed material and the frequencies of the entire machine tool.

- Increasing the stiffness of the interface can enhance the natural frequency of the entire machine tool within a certain range. When the arrangement and number of springs remain unchanged, increasing the interface

stiffness can effectively raise the machine's natural frequencies. As interface stiffness increases, the natural frequencies of the entire machine tool also rises accordingly; however, the rate of increase gradually diminishes.

In summary, modeling and simulation analysis of machine tool using the equivalent analysis method of interface spring-damping elements can optimize the structure and performance of CNC cylindrical grinding machines, thereby improving machining accuracy and stability. This is of great significance in meeting the requirements of modern high-efficiency, high-speed, and high-precision machining. Future research can further explore the impact of different joint parameters on machine tool performance and optimize the design and manufacturing of the machine tool.

It is noted that this research is supported by Undergraduate-postgraduate Integrated Curriculum Development Project. Through this project, undergraduate students, who plan to receive postgraduate education, can be exposed to real engineering application problems like what presented in this work beforehand, and try to conduct their own research to deal with these problems. It helps them to make a quick role change from student learning knowledge at the undergraduate level, to researcher applying knowledge at the postgraduate level.

Funding

This research is supported by Undergraduate-postgraduate Integrated Curriculum Development Project (No. BY202406) and 2023 Shanghai Education Commission Young Teacher Training Subsidy Program.

Conflicts of interest

The authors declare no conflict of interests.

Data availability statement

The datasets used or analyzed during the current study are available from the corresponding author on reasonable request.

Author contribution statement

All authors contributed to the study conception and design. Material preparation, data collection, and analysis were performed by Mingzheng Qi and Yang Guo. The first draft of the manuscript was written by Han Wang and Xinzhi Sun. All authors commented on previous versions of the manuscript. All authors read and approved the final manuscript.

References

1. V. Singh, M. Law, Machine tool multibody dynamic model updating using vision-based modal analysis[J], *Manufac. Technol. Today* **22**, 23–28 (2023)
2. S. Liu, W. Zheng, Priority order recognition method of module redesign for the CNC machine tool product family to improve green performance[J], *Trans. Canadian Soc. Mech. Eng.* **45**, 513–531 (2021)
3. H. Guo, J. Zhang, P. Feng et al., A virtual material-based static modeling and parameter identification method for a BT40 spindle-holder taper joint [J], *Int. J. Adv. Manufac. Technol.* **81**, 307–314 (2015)
4. K. Wang, C. Yang, Structural design optimization of movable-column horizontal machining center based on integral stiffness analysis and sensor measurement[J], *Sensors Mater. Int. J. Sensor Technol.* **35**, 4 (2023)
5. Y. Chang, J. Ding, H. Fan et al., Interfacial micromechanics modeling for bolted joints in ultra-precision machine tools, *J. Mech. Sci. Technol.* **37**, 4179–4191 (2023)
6. K. Okamura, T. Matsubara, K. Akada, Transient response analysis of hydraulic feed system of machine tool[J], *J. Japan Soc. Precision Eng.* **37**, 666–671 (1971)
7. M. Yoshimura, Optimal design in the product planning phase (Optimal Design, F14 Planning of the Mechanical Mechanics, Measurement and Control Division) [M]. 2017
8. C. Dogariu, D. Bardac, Prediction of the structure dynamic behavior of high speed turning machine spindles[J], *Applied Mech. Mater.* **555**, 3201 (2014)
9. R. Chen, X. Wang, C. Du et al., Stiffness model and experimental study of hydrostatic spindle system considering rotor swing. *Shock Vibration*[J] 5901432 (2020)
10. B. Revanasiddesh, A. Taj, N. Kumar et al., Extraction of modal parameters of CNC lathe bed using finite element and experimental method[J], *Mater. Today Proc.* **24**, 398–405 (2020)
11. T. Guo, L. Meng, X. Hua et al., Research on the dynamic identification method of weak parts in cantilever structures [J], *Sci. Prog.* **104**, 28988–29003 (2021)
12. K. Liu, J. Liu, L. Wang, Y. Zhao, F. Li, A modified model for identifying the characteristic parameters of machine joint interfaces[J], *Appl. Sci.* **13**, 11680 (2023)
13. S. Wu, W. Lei, T. Yu, Z. Dong, T. Liu, Effect of the stiffness of the turntable bearing joint on the dynamic characteristics of the five-axis machine tool rotary system[J], *Machines* **11**, 389 (2023)
14. Z. Gao, Y. Zhang, Y. Xi et al., Investigation of normal dynamic contact stiffness and damping characteristics in mixed lubrication for non-gaussian rough surfaces[J], *Mech. Solids* **58**, 2144–2161 (2023)
15. G. Song, C. Li, C. Liu et al., Modeling and analysis of nonlinear dynamics of machine tool sliding guide[J], *Nonlinear Dyn.* **112**, 8171–8197 (2024)
16. H. Huynh, Y. Altintas, Multibody dynamic modeling of five-axis machine tool vibrations and controller[J], *CIRP Ann.* **71**, 325–328 (2022)

Cite this article as: Mingzheng Qi, Han Wang, Xizhi Sun, Tianjian Li, Yang Guo, Tao Wu, Simulation and optimization of CNC cylindrical grinder Performance based on equivalent analysis of joints spring-damping characteristics, *Int. J. Metrol. Qual. Eng.* **16**, 4 (2025), <https://doi.org/10.1051/ijmqe/2025002>